


Osteoarthritis and Cartilage (2000) 8, 426–433

© 2000 Osteoarthritis Research Society International

doi:10.1053/joca.2000.0318, available online at <http://www.idealibrary.com> on 

1063–4584/00/060426+08 \$35.00/0

Osteoarthritis and Cartilage

Journal of the OsteoArthritis Research Society International



A technique for 3D *in vivo* quantification of proton density and magnetization transfer coefficients of knee joint cartilage

J. Hohe*†, S. Faber‡, T. Stammberger†, M. Reiser‡, K.-H. Englmeier† and F. Eckstein*

*Musculoskeletal Research Group, Institute of Anatomy, Ludwig-Maximilians Universität München, Pettenkoferstr. 11, D-80336 München, Germany

†Institut für Medizinische Informatik und Systemforschung, GSF Forschungszentrum, Neuherberg, Ingolstädter Landstr. 1, D-85764 Oberschleissheim, Germany

‡Institut für Klinische Radiologie, Klinikum der LMU München (Grosshadern), Marchioninistr. 15, D-81377 München, Germany

Summary

Objective: To develop an MR-based method for the *in vivo* evaluation of the structural composition of articular cartilage.

Design: Five sagittal magnetic resonance imaging (MRI) protocols were acquired throughout the knee joint of 15 healthy volunteers and the boundaries of the cartilage segmented from a previously validated sequence with high contrast between cartilage and surrounding tissue. The other sequences were matched to these data, using a 3D least-squares fit algorithm to exclude motion artefacts. In this way secondary images were computed that included information about the proton density (interstitial water content) and the magnetization transfer coefficient (macromolecules, collagen). The average signal intensities of the 3D cartilage plates were extracted from these data sets and related to a phantom.

Results: The signal intensity data showed a high interindividual variability for the proton density (patella 31%, lateral tibia 36%, medial tibia 29%); the patella displaying higher values than the tibia ($P < 0.001$). There were high correlations between the three plates. The magnetization transfer coefficient also showed high variability (patella 25%, lateral tibia 32%, medial tibia 30%) with the lowest values in the medial tibia ($P < 0.01$) and lower correlations between the plates. The slice-to-slice variation (medial to lateral) ranged from 9% to 24%.

Conclusion: An MR-based method has been developed for evaluating the proton density and magnetization transfer of articular cartilage *in vivo* and observing systematic differences between knee joint cartilage plates. The technique has the potential to supply information about the water content and collagen of articular cartilage, in particular at the early state of osteoarthritic degeneration. © 2000 Osteoarthritis Research Society International

Key words: Articular cartilage, Proton density, Magnetization transfer, Magnetic resonance imaging.

Introduction

Degenerative joint disease [osteoarthritis (OA)] is one of the most prevalent disorders: based on radiographic criteria,^{1,2} it affects most individuals above the age of 65. The costs involved have been estimated to amount to \$65 billion in the United States alone in 1992³ and are expected to reach 1% of the gross national product in the year 2000.⁴ In terms of diagnosis and prevention of OA, it is therefore important to search for suitable parameters that indicate damage to the cartilage at its earliest stage, when there is still maximum potential for successful therapeutic intervention. MRI supplies the unique opportunity to study the characteristics of articular cartilage non-invasively, making it feasible to collect systematic data from healthy individuals and patients, in both cross-sectional and longitudinal studies.^{5,6}

Quantitative MR based approaches for the assessment of articular cartilage have so far focused on morphological parameters, such as cartilage volume and thickness, as potential indicators of tissue loss in degenerative joint disease.^{7–14} However, a general drawback of this approach is that the cartilage has already been seriously damaged when morphological changes become detectable, whereas the earliest signs of OA involve structural and biochemical changes of the cartilage tissue, resulting in an altered composition of its main constituents, proteoglycans, collagens, interstitial water content,^{15–18} and others.

Previously, a number of attempts have been made to demonstrate a quantitative relationship between the signal intensity of the articular cartilage displayed in MR images and its microstructural/biochemical composition. Paul and co-workers,¹⁹ for instance, reported a correlation between the signal intensity variations throughout the cartilage in spin echo sequences and the proteoglycan distribution. More recently, Bashir and co-workers^{20,21} and Allen *et al.*²² suggested that gadolinium diethylenetriaminepentaacetic acid-enhanced MR imaging can be used for assessing the glycosaminoglycan content of normal and degenerated articular cartilage *in vivo*, and Insko *et al.*²³ have used

This study has been supported by the Deutschen Forschungsgemeinschaft (DFG).

Address correspondence to: Jan Hohe, Musculoskeletal Research Group, Institute of Anatomy, Pettenkoferstr. 11, D-80336 München, Germany. Tel: 49 89 3187 4191; Fax: 49 89 3187 4243; E-mail: jan_hohe@write.me

sodium imaging for the same purpose. Wolff and co-workers²⁴ evaluated the magnetization transfer (MT) contrast of human knee joint cartilage. The MT is generated by irradiating the macromolecular protons in the tissue with a low power off-resonance radio-frequency field, which results in a decreased water proton signal intensity in regions with tight magnetic coupling between water and macromolecules. It has been shown^{25,26} that the collagen macromolecules (not the proteoglycans) are the predominant determinants for this decrease of the signal intensity, indicating that it may be feasible to gain specific information about the collagen by extracting the MT effect from MR images obtained with and without an MT pre-pulse.^{6,27} The water content of the cartilage can, for instance, be assessed by determining T2 maps,²⁸ alternatively, Selby and co-workers²⁹ have developed a technique for assessing the proton density of knee joint cartilage from various gradient echo sequences with different echo times and flip angles. They found a good agreement with a direct measurement of the weight fraction of interstitial water in cartilage specimens. However, to date there exists no established technique for a quantitative and comprehensive evaluation of the structural cartilage composition under *in vivo* conditions throughout entire cartilage plates, independent of a specific section orientation. A 3D technique of image acquisition and analysis is particularly relevant in longitudinal studies, in which it is impossible to reproduce identical sectional images at precisely the same location.^{7,8,11,12} The possibility of longitudinally and quantitatively assessing structural changes of joint disease is not only important for the early diagnosis of cartilage lesions, but can also improve the objective evaluation of the effectiveness of various types of chondroprotective treatment, which aim to stop or slow down the degenerative process.¹⁷

The objective of this paper was thus to develop a quantitative, three-dimensional MR-based technique for the structural characterization of articular cartilage in the living. Specifically, we aimed to quantitatively assess the proton density and MT throughout the patellar and the medial and lateral tibia cartilage, gaining potential information on the cartilage water content and collagen. Using clinical MRI scanners, however, the time required for imaging entire joints with multiple sequences is relatively long, and artefacts can result from slight movements of the knee during imaging. We will demonstrate that this problem can be solved by using a semi-automated 3D matching algorithm that compensates translations and rotations of the knee joint between the different pulse sequences.

Material and methods

The technique proposed includes the following steps:

- (1) MR image acquisition.
 - (a) Image data acquisition using a previously validated MR sequence for determining the anatomically accurate outline of the cartilage [Fig. 1(a)].
 - (b) Acquisition of primary images for calculating the proton density and MT coefficient together with a phantom [Fig. 1(a–c)].
- (2) Segmentation and 3D matching.
 - (a) Segmentation of the cartilage outline from the image data obtained in step 1a [Fig. 1(a)], and 3D reconstruction of the entire cartilage plate (Fig. 2).
 - (b) 3D matching (if necessary) of the sequences obtained in step 1b to the segmented data set obtained in step 2a (Fig. 1).
- (3) Calculation of the proton density and MT coefficient.
 - (a) Calculation of secondary images (proton density and MT coefficient) from the primary images that are obtained in step 1b, and matched to each other in step 2b.
 - (b) 3D analysis of the signal intensity for the reconstructed patellar and tibial cartilage plates (obtained in step 2a) from the secondary image data (obtained in step 3a).
 - (c) Peeling of the peripheral rows of voxels throughout the 3D cartilage plate and normalization of the average cartilage signal intensity to the phantom.

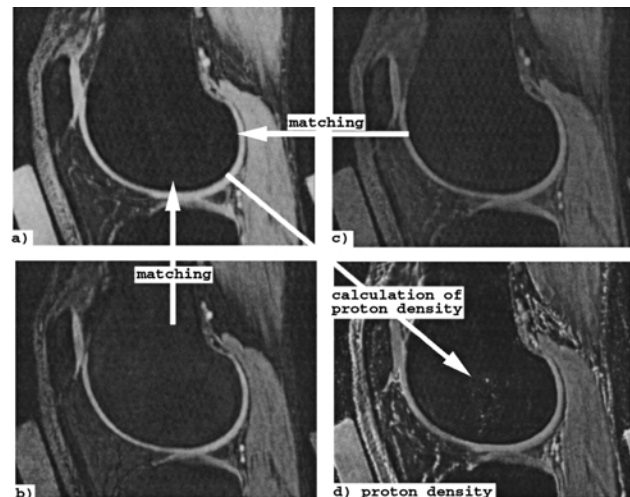


Fig. 1. Matching of the primary image (a–c) to the validated protocol in which the cartilage has been segmented (a), for calculating secondary images that include information about the proton density [water content, (d)].

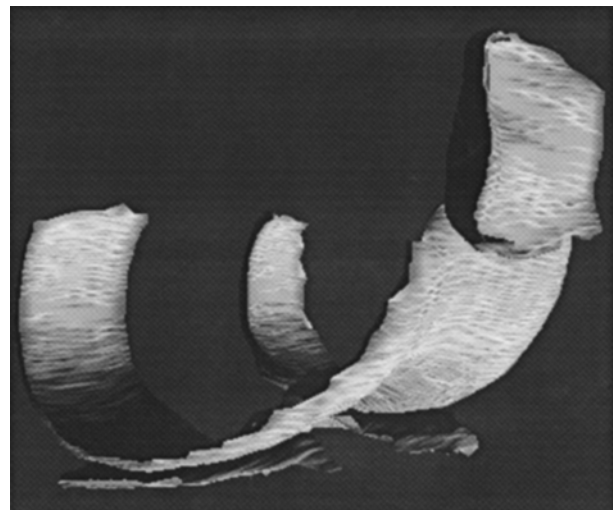


Fig. 2. 3D reconstruction of the patellar, tibial (and femoral—not analysed) cartilage plates for the integral signal intensity analysis, independent of specific section orientation and angulation.

AD 1. 3D IMAGE ACQUISITION

Fifteen volunteers (eight females, age 23.5 ± 3.9 years, and 7 males, age 24.8 ± 3.9 years) without disorders of the musculoskeletal system or previous trauma to the knee were imaged with a standard clinical 1.5 T MR scanner (Magnetom Vision, Siemens, Erlangen, Germany) with a slice thickness of 3 mm (sagittal orientation). The original in plane resolution was 0.62 mm^2 (matrix 256^2), but was interpolated to 0.31 mm^2 by zero-filling before fast Fourier transformation (sinc interpolation).³⁰ The knees of the volunteers were fixed in a collar and remained static in the magnet during all following protocols, in order to reduce motion artefacts as far as possible. Image acquisition was with three-dimensional spoiled gradient echo sequences (FLASH 3D; No Acq=1) with and without spectral fat-suppression (fs). The echo time (TE), flip angle (FA) and repetition time (TR) were varied as described by Selby and co-workers,²⁹ to compute secondary images of proton density (protocols 1–3). Protocols 4 and 5 served to obtain secondary images of the magnetization transfer effect (MT coefficient Ad 3).

- (1) TR₁: 59 ms, TE₁: 6 ms, FA₁: 12°, fs (protocol for segmentation)
- (2) TR₂: 59 ms, TE₂: 6 ms, FA₂: 40°, fs
- (3) TR₃: 59 ms, TE₃: 12 ms, FA₃: 40°, fs
- (4) TR₄: 42 ms, TE₄: 6 ms, FA₄: 12°
- (5) TR₅: 42 ms, TE₅: 6 ms, FA₅: 12°+magnetization transfer pulse

The total imaging time for acquiring the five sequences was approximately 35 min.

AD 2. SEGMENTATION AND 3D MATCHING

To perform the segmentation of the patellar and tibial cartilage we used the protocol with the highest contrast between the cartilage and the surrounding tissue (protocol 1), which, in previous studies, has been shown to produce accurate results for cartilage volume and thickness in comparison with surgically removed tissue,^{7,9} anatomical sections,^{8,10} CT arthrography,^{10,12} A-mode ultrasound,¹⁰ and stereophotogrammetry.¹⁴ The femoral cartilage was not analysed in the present study because its relatively thin cartilage, large surface area and complex geometry increased the relative effect of the movement artefacts. This made correct superimposition of the primary images difficult and did not leave enough interpretable information after the peeling of the two peripheral rows of voxels (see below). The segmentation of the patella and tibia was performed on a section-by-section basis with an interactive B-spline Snake (deformable contours) algorithm³¹ and was controlled visually in each image [Fig. 1(a)]. Because the segmentation of the cartilage in protocol 1 often did not correspond precisely with the outline of the cartilage in the other four sequences (due to the extended acquisition time and slight motion of the knee between protocols), we employed a semi-automated least-squares fitting algorithm for mapping the other sequences to the first data set (including the segmented cartilage area, Fig. 1). We observed that the described artefacts result predominantly from a translation and/or rotation of the image set within slices. The procedure of fitting one consecutive image set to the other was therefore performed by interactively defining corresponding points in both data sets, $\{\vec{x}_1, \vec{x}_2, \dots, \vec{x}_N\} \rightarrow \{\vec{y}_1, \vec{y}_2, \dots, \vec{y}_N\}$ where N is the number of defined

points, and by calculating the least-squares of the distances between the points (rotating and translating one point set in relation to the other). We then searched for the rotation and translation that maps the 3D-point set $\{\vec{x}_i\}$ to the point set $\{\vec{y}_i\}$, $i=1, 2, \dots, N$, by minimizing the sum of squares of the absolute differences between each pair of points.

$$\min \left\{ \sum_{i=1}^N \|\vec{y}_i - (R_{\min} \vec{x}_i + T_{\min})\|^2 \right\} \quad (1)$$

where R_{\min} and T_{\min} represent the rotation and translation matrix that solve (1). The method for calculating R_{\min} and T_{\min} was developed based on the work of Arun and co-workers³² and comprised the following steps:

- (a) Translation of the centroid \vec{c}_x of $\{\vec{x}_i\}$, and \vec{c}_y of $\{\vec{y}_i\}$ to the origin
- (b) Calculation of R_{\min}
- (c) Calculation of $T_{\min} = \vec{c}_y - R_{\min} \vec{c}_x$.

The most important part of the calculation was performed in step B, the rotation matrix R_{\min} was being found by computing the singular value decomposition (SVD) of H .

$$H = \sum_{i=1}^N (\vec{y}_i - \vec{c}_y)(\vec{x}_i - \vec{c}_x)^t = U \Lambda V^t \quad (2)$$

where U , Λ , V represent the SVD of H . In this case U and V are 3×3 orthonormal matrices and Λ is a diagonal 3×3 matrix with the positive or zero singular values. It has been shown previously that the orthonormal matrix $X = VU^t$ represents the searched R_{\min} , if X is a rotation matrix ($\det(X) = 1$).³² Using this algorithm, we were able to gain the information necessary for reducing the motion artefacts of the volunteers during the MRI scanning procedure. Please note that only few corresponding points need to be selected in some of the images, but that the translation and rotation is then automatically performed for the entire 3D data set. It is essential for the accuracy of the matching that the corresponding points are selected correctly. As a tool for defining appropriate image points and for demonstrating the effectiveness of the matching, corresponding slices of two different data sets were superimposed to one image, the original sets being displayed in different colors. This was achieved by manipulating the color components (red, green, blue), but not the signal intensity of the data sets. In practice, areas of high signal intensity correspond to the outlines of the cartilage plates in T1-weighted fat-suppressed images; if these do not overlap exactly edges (with one of the original colors) occur where the two components do not merge. These original colored edges also become visible at the cartilage surface of the non fat-suppressed images of protocol 4 and 5. This information can be used to visually assess the necessity for the matching, to demonstrate its effectiveness, and to improve its quality, if not satisfactory. In order to exclude residual artefacts at the cartilage edges, the peripheral two rows of voxels were excluded from the signal intensity analysis.

AD 3. CALCULATION OF THE PROTON DENSITY (PD) AND MAGNETIZATION TRANSFER (MT) COEFFICIENT

Based on the technique described by Selby *et al.*,²⁹ we matched protocols 1–3 and created secondary images of

proton density, combining them on a voxel-by-voxel basis according to the expression:

$$S_{pd} = \left(\frac{S_1 S_2 a}{S_2 b - S_1 c} \left(\frac{S_2}{S_3} \right)^{(TE_1 / (TE_3 - TE_1))} \right) \quad (3)$$

S_1 , S_2 and S_3 are the signal intensities of the pixels of the protocols 1, 2 and 3 described in the section 'Data Acquisition'. The values of a , b and c result from the flip angles (FA_i) of the three MRI protocols: $a = \cos FA_1 - \cos FA_2$, $b = \sin FA_1 (1 - \cos FA_2)$, $c = \sin FA_2 (1 - \cos FA_1)$ (Fig. 1).

These values were finally related to a copper-sulfate phantom present in the images, in order to normalize S_{pd} and to be able to compare the results among different volunteers. This phantom has the advantage that its signal intensity characteristics are particularly stable, and this was verified by demonstrating that the ratios between the signal intensity of the muscles and those of the phantom did not show any systematic decrease or increase over the period of data acquisition in the volunteers. Please note that the phantom consisted of an agarose gel and not of pure water, its relaxation parameters being more similar to human tissue than those of a water phantom.

Based on the findings of Kim and co-workers,²⁵ protocols 4 and 5 were used for calculating secondary images of the MT coefficient.³³ Since the cartilage–bone interface cannot be accurately located in images without fat-suppression,³⁴ we used defined points on the cartilage surface to match protocol 4 and 5 to the validated segmentation of protocol 1, which precisely describes the outline of the cartilage.^{7–10,12,14} To extract the MT coefficient, the signal intensity of protocol 5 (with magnetization transfer) was subtracted from protocol 4, and normalized by dividing it through the signal intensity of protocol 4.³³ Please note that in this case the results are normalized to protocol 4 and given as a percentage, making a standardization of the signal intensity values vs the phantom unnecessary.

$$MT_{\text{coefficient}} = \frac{S_4 - S_5}{S_4} \times 100 \quad (4)$$

It is important to realize that the global results for the signal intensity (SI) are given for the entire 3D cartilage plates of the patella, medial tibia and lateral tibia (Fig. 2, 3D reconstruction), both for the proton density and the MT coefficient. Differences between the volunteers were tested for statistical significance with the paired t -tests.

In order to provide an estimate of the slice-to-slice variation of PD and MT across the cartilages, we determined the average coefficient of variation (CV%) of the slices within each plate of each volunteer (standard deviation divided by the mean*100) and related this slice-to-slice variation to the interindividual variability (given as the CV% between individuals). To evaluate systematic changes of PD and MT throughout different regions, we compared slices within the lateral (second slice from lateral), the middle, and the medial aspect (penultimate slice from lateral) of each plate. Systematic differences were again evaluated with the paired t -test.

The correlation between different plates and between the PD and MT in each plate was assessed with regression analysis. Differences in these two parameters between men and women were analysed with the Mann–Whitney U-test.

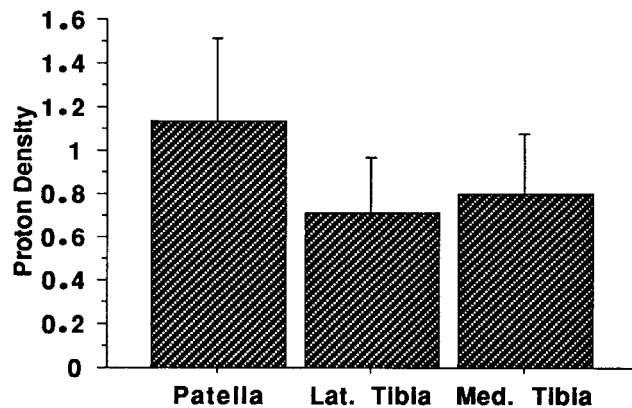


Fig. 3. Proton density of the patella, medial and lateral tibia in 15 volunteers: The data show a high interindividual variability (error bars indicate 1 standard deviation), and a systematic difference between the patella and tibia ($P < 0.001$).

Results

PROTON DENSITY OF THE PATELLAR AND TIBIAL CARTILAGE

The proton density of the patellar cartilage (1.07 ± 0.34) was found to be significantly higher than that of the tibial cartilage ($P < 0.001$), whereas the medial (0.74 ± 0.21) and lateral tibia (0.71 ± 0.25) did not show significant differences (Fig. 3). The data displayed a high interindividual variability among the volunteers (patella: CV% = 31%; lateral tibia: 36%; medial tibia: 29%; Fig. 3). However, individuals with a high proton density of the patellar cartilage generally also displayed relatively high values in the tibia, the correlation (r) between the patella and the lateral tibia being 0.93, that between patella and medial tibia 0.78, and that between the medial and lateral tibia 0.82 (level of significance < 0.001). There was no significant difference between the male and female volunteers.

The slice-to-slice variation (medial to lateral) of the PD was lower than the interindividual variation, the values being 9% in the patella, 19% in the lateral tibia, and 10% in the medial tibia. The variability of the lateral tibia was significantly higher than that of the patella ($P < 0.01$) and that of the medial tibia ($P < 0.05$). In the patella, the lateral slice showed a significantly lower PD (0.97 ± 0.36) than slices obtained in the middle (1.19 ± 0.41 ; $P < 0.001$) and in the medial patellar facet (1.15 ± 0.40). In the medial and lateral tibia, however, no significant difference was observed between medial, middle and lateral slices.

MT COEFFICIENTS OF THE PATELLAR AND TIBIAL CARTILAGE

The MT coefficients of the patella (15.4 ± 3.8) and lateral tibia (15.3 ± 4.9) were significantly ($P < 0.01$) higher than those of the medial tibia (11.8 ± 3.6) (Fig. 4). The MT values also displayed a relatively high interindividual variability (patella: 25%; lateral tibia: 32%; medial tibia: 30%; Fig. 4). The correlation coefficients between the patella and the lateral tibia were 0.56 ($P < 0.05$), that between patella and medial tibia 0.32 (not significant), and that between the medial and lateral tibia 0.0 (not significant). There was no significant difference between the male and female volunteers.

In the tibia, the slice-to-slice variation (medial to lateral) of the MT was lower than the interindividual variation, the values being 19% in the lateral tibia and 12% in the medial

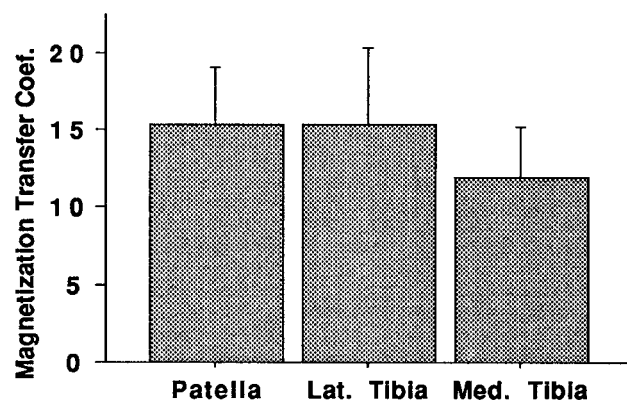


Fig. 4. MT coefficient of the patella, the medial and lateral tibia in 15 volunteers. The data show a high interindividual variability (error bars indicate 1 standard deviation), and a systematic difference between the medial and lateral tibia ($P < 0.01$).

tibia. In the patella, however, the intracartilage variation (29%) was significantly higher than in the medial tibia ($P < 0.001$) and was similar to the interindividual variability. In the patella, the lateral slice showed a significantly higher MT (16.8 ± 4.2) than the middle (14.2 ± 2.8 ; $P < 0.05$), but the medial slice (16.3 ± 6.1) was not significantly different. In the lateral tibia, the medial slice (13.0 ± 5.3) displayed a significantly lower MT than the middle (15.7 ± 3.9) and the lateral slice (17.8 ± 9.9), the level of significance being $P < 0.01$ and 0.05 , respectively. In the medial tibia, however, no significant difference was observed between medial, middle and lateral slices.

CORRELATION BETWEEN PROTON DENSITY AND MT COEFFICIENTS

There was no significant correlation between the proton density and MT coefficient in the patella ($r = -0.01$) and lateral tibia ($r = -0.19$), but a significant association between the two parameters in the medial tibia ($r = +0.68$; $P < 0.05$).

Discussion

The aim of this study was to develop a quantitative, three-dimensional technique for the *in vivo* quantification of articular cartilage MR signal intensity. Specifically, we have assessed the proton density and MT throughout the cartilage plates of the human knee joint to gain insight into the structural composition of articular cartilage. This is an extension of a previously described morphometrical analysis^{7,8,10,12,13,30} that focused on cartilage volume and thickness as potential parameters for characterizing the state and progression of osteoarthritic disease. The technique developed here may allow non-invasive detection of cartilage lesions at an earlier stage, when there is still maximum potential for effective therapeutic intervention.¹⁷

METHODOLOGICAL ASPECTS

In order to be able to extract relevant data concerning the proton density and MT of the knee joint cartilage plates, several methodological problems had to be solved. To quantitatively determine the proton density and the MT

coefficient from the raw MRI data, the cartilage regions of interest have to be defined. We therefore selected an MR sequence, which has been previously validated in terms of accurate assessment of cartilage volume and thickness, for determining the anatomically accurate outline of the cartilage. For the interactive segmentation we applied a B-spline Snake algorithm³¹ that has been shown to be superior to manual segmentation.

The primary image data for estimating the proton density and MT coefficient of the cartilage were obtained according to the descriptions of Selby *et al.*²⁹ and Faber *et al.*³³ These authors have suggested that the MR signal intensity of secondary images (obtained from merging several primary images) reflects the water content and collagen of the articular cartilage. Using a compression apparatus for investigating the *in situ* deformation of articular cartilage in intact joints,^{35,36} Faber *et al.*³³ have demonstrated that the proton density shows a substantial decrease upon cartilage compression (consistent with loss of interstitial water from the proteoglycan–collagen matrix), whereas the MT coefficient displays a considerable increase (consistent with a closer packing of the collagen fibrils in the compressed cartilage matrix).

For cross-sectional and longitudinal studies in patients or volunteers, the analysis of the MR signal intensity should not rely on single sections, since these are intrinsically difficult to define and to reproduce.^{7,8,11} We therefore applied a 3D imaging protocol covering the entire knee joint, in order to be able to extract the average proton density and MT coefficients for entire 3D cartilage plates, these values being independent of a specific section position or angulation. Presently, this type of analysis allows for a global assessment of the cartilage plate, but not yet for determining focal changes which may occur in the earliest stage of the disease. However, in future work we intend to map the spatial distribution of PD and MT throughout various anatomic regions of the cartilage plates as well as throughout various cartilage layers (superficial, middle, deep), and then to use 3D registration algorithms to directly compare the differences between the signal intensity patterns obtained at different points in time.³⁷ In this way, focal changes may be demonstrated directly, independent of the specific section location.

The use of 3D imaging sequences naturally involves relatively long imaging times, and under *in vivo* conditions it is difficult to keep the object of interest entirely stationary during imaging. Despite our efforts to keep the knee joints fixed and to use specialized image protocols that have been optimized for acquiring 3D data with high spatial resolution at minimal imaging times,^{30,38} the digital image analysis revealed that various degrees of rotation and translation had occurred between the acquisition of the various sequences required for computing the secondary images. We therefore had to establish an efficient technique for correcting these motion artefacts. This was achieved by applying a semi-automated approach based on a least-squares fitting algorithm that allows the primary data sets to be matched with the image data, in which segmentation of the entire cartilage plate of interest has been carried out. This implies that segmentation (which is the most time-consuming step) needs to be performed in only one of the data sets, and that the signal intensities of the secondary images can be immediately computed from the data matched to the first protocol. We have created a tool for indicating the necessity and demonstrating the effectiveness of the matching, by superimposing corresponding slices of different data sets onto one image, the

original images being displayed in different colors. The occurrence of one of the two original colors at the edges of the cartilage plates indicates that matching is required and the same effect can be used to control its efficiency. We observed satisfactory results throughout all patellar and tibial cartilage plates of the 15 volunteers after applying the matching algorithm, and in order to exclude residual artefacts at the cartilage edges (resulting, for instance, from partial volume effects) the peripheral two rows of voxels were excluded from the signal intensity analysis. However, due to its large surface area, thin cartilage layer and complex geometry, the femoral cartilage did not yield satisfactory results. For this reason we dispensed with analysing the distal femur in the present study, which is a shortcoming. However, if the motion artefacts can be reduced and/or the resolution increased, it will become feasible to assess femoral cartilage with this method.

By normalizing the secondary data sets of the proton density to a phantom, we ensured comparability among different volunteers independent of the specific imaging conditions. Please note that we used a copper-sulfate phantom consisting of an agarose gel and not of pure water, because not only the protocols given here, but a variety of other MR-sequences, were acquired. The addition of agarose to water may have changed the amount of free water in the phantom. Only free water has T2 values large enough to receive a signal with standard pulse sequences. Therefore we assume that only the spin density of the free water fraction of the phantom was measured by our method. This may explain why some cartilage samples showed larger spin density values than the phantom, and future studies will have to address whether this shortcoming can be overcome by using a pure water phantom.

RESULTS FOR PROTON DENSITY AND MT COEFFICIENT

The high interindividual differences in both the proton density and MT coefficient are consistent with results reported in the literature addressing cartilage biochemistry¹⁶ and mechanical properties.^{39,40} It is interesting to observe systematic differences between various cartilage plates, indicating differences in their structural composition. Such differences have also been observed in biochemical *in vitro* studies.^{39,41} Froimson *et al.*⁴¹ reported that the water content was highest in the patellar cartilage, a finding that is reproduced in our study.

The findings indicate that there exist systematic variations of PD and MT even within individual cartilage plates of healthy volunteers, and these may relate to differences of the mechanical loading characteristics, e.g. of the lateral and medial patellar facet, or of those parts of the tibia which are covered by the menisci vs those that are not.

The relatively low correlation of the proton density and MT coefficients within the same cartilage plates suggests that both parameters provide independent information with regard to cartilage composition and properties.

POTENTIAL APPLICATIONS AND FUTURE DEVELOPMENTS

Further *in vivo* studies will have to substantiate whether the proton density and MT coefficients vary with age and disease states. The technique presented makes it possible to analyse whether functional adaptation of articular cartilage to mechanical stimuli can be observed on a structural

level, for instance by comparing these parameters in individuals subjected to different levels and types of physical exercise. In particular, future studies will have to demonstrate whether the technique can be used to characterize the mechanical properties of the tissue, and to detect and monitor degenerative cartilage changes before the state of tissue loss. In this context it may also be of high interest to collect quantitative data on the proteoglycans, which represent an important constituent of the articular cartilage. It should be stressed that the post-processing technique presented in this study is not confined to the use of specific imaging protocols, but can be readily applied to alternate MRI sequences, for instance those proposed by Bashir and co-workers^{20,21} and Insko *et al.*²³ for measuring the proteoglycan content, or those for calculating T2 maps.²⁸ An important step will be to extend the present technique to allow for regional analyses, both perpendicular and parallel to the cartilage surface, and to the analysis of focal rather than global changes. Since cartilage properties and biochemistry have been shown to vary with tissue depth and in the peripheral vs central aspects of the joint surface,^{17,42} such a technique may allow analysis of the inhomogeneous structure of the cartilage *in vivo*, under both physiological and pathological conditions. This will, however, require image acquisition at a higher spatial resolution, the development of faster MR sequences being particularly important in this context. In this way it should become possible to reduce the imaging time and potential motion artefacts and to avoid the elimination of peripheral voxels, allowing for the analysis of the signal intensity distribution at the cartilage surface, compared with deeper areas of the cartilage.

Acknowledgments

The study has been supported by the Deutsche Forschungsgemeinschaft (DFG). We would like to thank Verena Springer, Susanne Lukasz and Rohland Mühlbauer for their help with the data acquisition and segmentation. The work presented in this paper is part of the doctoral thesis (in preparation) of Jan Hohe at the Anatomischen Anstalt, Ludwig-Maximilians-Universität, München.

References

1. Felson DT. Epidemiology of hip and knee osteoarthritis. *Epidemiol Prev* 1988;10:1–28.
2. Felson DT. Osteoarthritis. *Rehum Dis Clin North Am* 1990;16:499–512.
3. Yelin E, Callaghan LF. The economic cost and social and psychological impact of musculoskeletal conditions. *Arthritis Rheum* 1995;38:1351–62.
4. Yelin E. The economics of osteoarthritis. In: Brandt K, Doherty M, Lohmander L, Eds. *Osteoarthritis*. Oxford: Oxford Medical Publishers 1998:23–30.
5. Recht MP, Resnick D. MR imaging of articular cartilage: current status and future directions. *AJR* 1994;163:283–90.
6. Peterfy CG, Genant HK. Emerging application of magnetic resonance imaging in the evaluation of articular cartilage. *Radiol Clin North Am* 1996;34:195–213.
7. Peterfy CG, van Dijke CF, Janzen DL, Gluer CC, Namba R, Majumdar S, et al. Quantification of articular cartilage in the knee with pulsed saturation transfer subtraction and fat-suppressed MR

- imaging: optimization and validation. *Radiology* 1994;192:485–91.
8. Eckstein F, Gavazzeni A, Sittek H, Haubner M, Lösch A, Milz S, et al. Determination of knee joint cartilage thickness using three dimensional magnetic resonance chondro-crassometry (3D MR-CCM). *Magn Res Med* 1996;36:256–65.
 9. Piplani MA, Disler DG, McCauley TR, Holmes TJ, Cousins JP. Articular cartilage volume in the knee: semiautomatic determination from three-dimensional reformations of MR images. *Radiology* 1996;198:855–9.
 10. Eckstein F, Adam C, Sittek H, Becker C, Milz S, Schulte E, et al. Non-invasive determination of cartilage thickness throughout joint surfaces using magnetic resonance imaging. *J Biomech* 1997;30:285–9.
 11. Eckstein F, Westhoff J, Sittek H, Maag K-P, Haubner M, Faber S, et al. In vivo reproducibility of three-dimensional cartilage volume and thickness measurements with magnetic resonance imaging. *AJR* 1998;170:593–7.
 12. Eckstein F, Schnier M, Haubner M, Priebisch J, Glaser C, Englmeier K-H, et al. Accuracy of cartilage volume and thickness measurements with magnetic resonance imaging. *Clin Orthop* 1998;352:137–48.
 13. Stammberger T, Eckstein F, Englmeier K-H, Reiser M. Determination of 3D cartilage thickness from MR imaging—computational method and reproducibility in the living. *Magn Reson Med* 1999;41:529–36.
 14. Cohen ZA, McCarthy DM, Arteshian GA, Kwak SD, Legrand P, Fogarasi F, et al. Knee cartilage topography, thickness, and contact areas from MRI: *in vitro* calibration and *in vivo* measurements. *Osteoarthritis Cart* 1999;7:95–109.
 15. Bollet AJ, Nance JL. Biochemical findings in normal and osteoarthritic articular cartilage II chondroitin sulfate concentration and chain length, water, and ash content. *J Clin Invest* 1966;45:1170–7.
 16. Kuettner KE. Biochemistry of articular cartilage in health and disease. *Clin Biochem* 1997;25:155–63.
 17. Buckwalter JA, Mankin HJ. Articular cartilage: degeneration and osteoarthrosis, repair, regeneration, and transplantation. *J Bone Joint Surg* 1997;79-A:612–32.
 18. Armstrong CG, Mow VC. Variations in the intrinsic mechanical properties of human articular cartilage with age, degeneration, and water content. *J Bone and Joint Surg* 1982;88–94.
 19. Paul PK, Jasani MK, Sebok D, Rakhit A, Dunton AW, Douglas FL. Variations in MR signal intensity across normal human knee cartilage. *J Magn Reson Im* 1993;3:569–74.
 20. Bashir A, Gray ML, Boutin RD, Burstein D. Glycosaminoglycan in articular cartilage: In vivo assessment with delayed Gd(DTPA)²⁻-enhanced MR imaging. *Radiology* 1997;205:551–8.
 21. Bashir A, Gray ML, Hartke J, Burstein D. Nondestructive imaging of human cartilage glycosaminoglycan concentration by MRI. *Magn Reson Med* 1999;41:857–65.
 22. Allen RG, Burstein D, Gray ML. Monitoring glycosaminoglycan replenishment in cartilage explants with gadolinium-enhanced magnetic resonance imaging. *J Orthop Res* 1999;17:430–6.
 23. Insko EK, Kaufman JH, Leigh JS, Reddy R. Sodium NMR evaluation of articular cartilage degradation. *Magn Reson Med* 1999;41:30–4.
 24. Wolff SD, Chesnick S, Frank JA, Lim KO, Balaban RS. Magnetization transfer contrast: MR imaging of the knee. *Radiology* 1991;179:245–9.
 25. Kim DK, Ceckler CL, Hascall VC, Calabro A, Balaban RS. Analysis of water-macromolecule proton magnetization transfer in articular cartilage. *Magn Reson Med* 1993;29:211–5.
 26. Aoki J, Hiraki Y, Seo GS, Shukunami C, Moriya H. Effect of collagen on magnetization transfer contrast assessed in cultured cartilage. *Nippon Igaku Hoshasen Gakkai Zasshi* 1996;56:877–9.
 27. Vahlensieck M, Dombrowski F, Leutner C, Wagner U, Reiser M. Magnetization transfer contrast (MTC) and MTC-subtraction: enhancement of cartilage lesions and intracartilaginous degeneration in vitro. *Skeletal Radiol* 1994;23:535–9.
 28. Frank LR, Wong EC, Luh WM, Ahn JM, Resnick D. Articular cartilage in the knee: mapping of the physiologic parameters at MR imaging with a local gradient coil—preliminary results. *Radiology* 1999;210:241–6.
 29. Selby K, Peterfy CG, Cohen ZA, Ateshian GA, Mow VC, Ross M, et al. In vivo MR quantification of articular cartilage water content: a potential early indicator of osteoarthritis. In: *Proceedings of the 3rd SMRM/ESMRMB, Nizza, France, 1995, 204. Abstract.*
 30. Eckstein F, Tieschky M, Faber S, Haubner M, Kolem H, Englmeier K-H, et al. Effects of physical exercise on cartilage volume and thickness *in vivo*—an MR imaging study. *Radiology* 1998;207:243–8.
 31. Stammberger T, Eckstein F, Michaelis M, Englmeier K-H, Reiser M. Interobserver reproducibility of quantitative cartilage measurements: comparison of B-spline snakes and manual segmentation. *Magn Res Imaging* 1999;64:1033–42.
 32. Arun KS, Huang TS, Blostein SD. Least-squares fitting of two 3-D point sets. *IEEE Trans Pattern Anal Machine Intell* 1987;9:698–700.
 33. Faber SC, Herberhold C, Stammberger T, Reiser M, Englmeier KH, Eckstein F. Quantitative changes of articular cartilage microstructure during compression of an intact joint. In: *Proceedings of the 7th SMRM/ESMRMB, Philadelphia, USA, 1999, 547. Abstract.*
 34. Eckstein F, Sittek H, Milz S, Putz R, Reiser M. The morphology of articular cartilage assessed by magnetic resonance imaging (MRI) reproducibility and anatomical correlation. *Surg Radiol Anat* 1994;16:429–38.
 35. Herberhold C, Stammberger T, Faber S, Putz R, Englmeier K-H, Reiser M, et al. A MR-based technique for quantifying the deformation of articular cartilage during mechanical loading in an intact cadaver joint. *Magn Res Med* 1998;39:843–50.
 36. Herberhold C, Faber S, Stammberger T, Steinlechner M, Putz R, Englmeier K-H, et al. In situ measurement of articular cartilage deformation in intact femoropatellar joints under static loading. *J Biomech* 1999;32:1287–97.
 37. Stammberger T, Hohe J, Englmeier K-H, Reiser M, Eckstein F. Elastic registration of 3D cartilage surfaces from MR image data for detecting local changes of the cartilage thickness. *Magn Res Med* 1999; in press.
 38. Tieschky M, Faber S, Haubner M, Kolem H, Schulte E, Englmeier K-H, et al. Repeatability of patella

- cartilage thickness patterns in the living, using a fat-suppressed MRI sequence with short acquisition time and 3D data processing. *J Orthop Res* 1997;15:808–13.
39. Athanasiou KA, Rosenwasser MP, Buckwalter JA, Malinin ZI, Mow VC. Interspecies comparison of *in situ* intrinsic mechanical properties of distal femoral cartilage. *J Orthop Res* 1991;9:330–40.
40. Eckstein F, Tieschky M, Faber S, Englmeier KH, Reiser M. Functional analysis of articular cartilage deformation, recovery, and fluid flow following dynamic exercise *in vivo*. *Anat Embryol* 1999;200:419–24.
41. Froimson MI, Ratcliffe A, Gardner RR, Mow VC. Differences in patellofemoral joint cartilage material properties and their significance to the etiology of cartilage surface fibrillation. *Osteoarthritis Cart* 1997;5:377–86.
42. Mow VC, Ratcliff A. Structure and function of articular cartilage and meniscus. In: Mow VC, Hayes WV, Eds. *Basic Orthopaedic Biomechanics*. Philadelphia: Lippincott-Raven 1997; 113–77.
-